Front. Environ. Sci. Eng. 2022, 16(7): 89
https://doi.org/10.1007/s11783-021-1497-0

RESEARCH ARTICLE

Preparation of reverse osmosis membrane with high permselectivity and anti-biofouling properties for desalination

Xinxia Tian[1], Hui Yu[1], Jun Yang[2], Xiaotai Zhang[1], Man Zhao[1], Yang Yang[1], Wei Sun[1], Yangyang Wei[1], Yin Zhang[1], Jian Wang (✉)[1], Zhun Ma (✉)[3]

1 The Institute of Seawater Desalination and Multipurpose Utilization, MNR (Tianjin), Tianjin 300192, China
2 Tianjin Huanke Environment Consulting CO., LTD, Tianjin 300191, China
3 College of Chemical and Biological Engineering, Shandong University of Science and Technology, Qingdao 266590, China

HIGHLIGHTS

- Nanoparticle incorporation and anti-biofouling grafting were integrated.
- Flux of modified membranes was enhanced without rejection sacrificing.
- Anti-biofouling property of modified membranes was improved.

GRAPHIC ABSTRACT

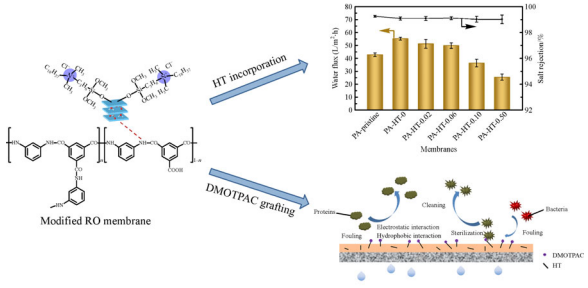

ARTICLE INFO

Article history:
Received 29 June 2021
Revised 18 October 2021
Accepted 22 October 2021
Available online 22 November 2021

Keywords:
Anti-biofouling grafting
Nanoparticle incorporation
Sterilization rates
Water flux
Water flux recovery

ABSTRACT

High performance is essential for the polyamide (PA) reverse osmosis (RO) membranes during the desalination process. Herein, RO membranes with high permselectivity and anti-biofouling properties were fabricated by nanoparticles incorporation and anti-biofouling grafting. Hydrotalcite (HT) incorporation was performed with a dual role, enhancing water flux and acting as grafting sites. The HT incorporation increased the water flux without sacrificing the salt rejection, compensating for the loss caused by the following grafting reaction. The exposed surface of HT acted as grafting sites for anti-biofouling agent dimethyloctadecyl[3-(trimethoxysilyl)propyl]ammonium chloride (DMOTPAC). The combination of HT incorporation and DMOTPAC grafting endowed RO membranes with high permselectivity and anti-biofouling properties. The water flux of the modified membrane PA-HT-0.06 was 49.8 L/m^2·h, which was 16.4% higher than that of the pristine membrane. The salt rejection of PA-HT-0.06 was 99.1%, which was comparable to that of the pristine membrane. As to the fouling of negatively charged lysozyme, the modified membrane's water flux recovery was superior to that of the pristine membrane (e.g. 86.8% of PA-HT-0.06 compared to 78.2% of PA-pristine). The sterilization rates of PA-HT-0.06 for *E. coli* and *B. subtilis* were 97.3% and 98.7%, much higher than those of the pristine membrane (24.0% for *E. coli* and 26.7% for *B. subtilis*).

1 Introduction

Water supply is strongly related to human health and social development. Drinking water shortages are important events in many regions and countries. The separation of clean water from unconventional water resources could provide solutions to these issues. Reverse osmosis (RO) has attracted wide attention for its extensive applicability in brackish water and seawater desalination. Thin-film composite (TFC) polyamide (PA) RO membranes consisting of a dense separating layer and a porous support layer have been the leading products of this field. However, relatively low permselectivity and membrane fouling limit

✉ Corresponding authors
E-mail: wangjian@isdmu.com.cn (J. Wang); mzyxy199@163.com (Z. Ma)

the widespread applicability of RO membranes (Fane et al., 2015).

The membrane performance determines the cost-efficiency of the RO process, affecting the promotion of RO technology in water treatment. Due to the inherent characteristics of the materials, PA RO membranes exhibit a permeability-selectivity trade-off relationship, and the performance has reached the upper limit of this technology (Yin and Deng, 2015). Moreover, the TFC RO membrane is inherently predisposed to fouling during the operation process, particularly in the presence of microorganisms, which can dramatically deteriorate the membrane performance (Díez et al., 2020). To obtain favorable TFC RO membranes with stable high performance, both the permselectivity and anti-biofouling properties of the membranes should be enhanced.

The synthesis of nanocomposite membranes has been proved to be an effective technology to combine the benefits of polymers and inorganic nanomaterials (Guo et al., 2019; Dai et al., 2022). Through shape-tailoring and control of the porous structures, nanotechnology endows membranes with high permselectivity. Hoek and his coworkers first adopted a new strategy of incorporating zeolite nanoparticles into the PA matrix to fabricate thin-film nanocomposite (TFN) RO membranes. In this way, they have enhanced the pure water permeability from 2.1 $\times$ 10^{-12} m/Pa/s to 3.8 $\times$ 10^{-12} m/Pa/s (Jeong et al., 2007). Various nanoparticles such as zeolites, graphene oxides, nanotubes and metal-organic frameworks have been employed for TFN RO membrane fabrication. Most studies indicated that incorporating an appropriate amount of nanoparticles could improve water flux without sacrificing salt rejection.

Layered nanoparticles, including montmorillonite and hydrotalcite, have been introduced into polymer matrix for nanocomposite membrane fabrication. Their unique structure is beneficial to the channel construction for separating components and improving membrane performance. It was stated that the layered nanoparticles montmorillonite in matrix constructed ionized water channel and water can transport through the hydrated channels, which enhanced the separation factor of the nanocomposite membranes (Gao et al., 2015). Hydrotalcite (HT) was dispersed in an aqueous solution and incorporated into the PA matrix in the interfacial polymerization step to construct transport channels for water in our previous study. The TFN RO membranes exhibited high permselectivity, and the water flux increased without sacrificing salt rejection (Tian et al., 2020).

As mentioned above, the native performance could be improved by fine-tuning the composition and structure. However, RO membranes are susceptible to fouling during the operation process, which would inevitably reduce the permselectivity and shorten the service life of the membranes (Zhao et al., 2018). Among all kinds of fouling, biofouling has been considered the most challenging obstacle to overcome because microorganisms widely exist in feed and multiply quickly on membrane surface to form a biofilm (Zhu et al., 2018). Conventionally, adding chemical reagents in the feed water and chemical cleaning of the membrane are the standard methods to restore the performance in the RO system (Henthorne and Boysen, 2015). However, these procedures could cause structural damage to the RO membranes (Kang et al., 2007). In addition, the residual viable microorganism could act as a precursor bringing about severe biofouling, and even the microorganisms could be removed by 99.99% (Flemming et al., 1997). Hence, to obtain favorable TFC RO membranes with prolonged and stable high performance, besides incorporating nanoparticles for high permselectivity, the membranes should be endowed with anti-biofouling property.

Membrane modification (including nanoparticle incorporation, surface coating and grafting) has been proved to be an efficient approach to prevent pollutants from adhesion or kill microorganisms (Zhao et al., 2018). Dispersing in an aqueous or organic solution, various nanoparticles could be introduced into the PA layer during interfacial polymerization to endow membranes with anti-biofouling properties (Chae et al., 2015). Nevertheless, the disadvantage of nanoparticle incorporation is that nanoparticles embedded in the PA matrix can not contact pollutants directly, which would inevitably reduce the anti-biofouling capacity. Surface coating has been used to impart efficient anti-biofouling properties to the membranes to ensure sufficient contacts between anti-biofouling agents and pollutants. Some polymers (e.g. biomaterials, copolymers, nanoparticles) could be adhered to membranes for anti-biofouling resistance improvement by surface coating. The surface coating could be a promising pathway to form an integrated layer protecting the membrane from biofouling. The disadvantage of this approach lies in the weak interaction between the coating layer and membrane surface, resulting in the destruction of the coating layer under hydraulic conditions (Hailemariam et al., 2020). In contrast, surface grafting can provide a strong chemical binding between protecting layer and the membrane surface. The anti-biofouling components on the membrane surface can contact sufficiently with pollutants to protect the functional layers. Moreover, the chemical bonds could provide strong interaction between functional components and membranes surface to protect the anti-biofouling agents from loss. Nevertheless, the bonds between functional components and membranes surface usually alter the cross-linked structure of the PA matrix, leading to rejection decline (Saeki et al., 2014).

Grafting anti-biofouling agents on nanoparticles embed in the PA matrix could be an efficient strategy to endow RO membranes with anti-biofouling properties without damaging the PA matrix. As previously mentioned, HT nanoparticles have been proved to be promising alternatives to increase membrane permselectivity (Tian et al.,

2020). Meanwhile, HT nanoparticles contain abundant hydroxyls, which can react with siloxy of silane coupling agents, allowing for ant-biofouling grafting (Tian et al., 2020). Consequently, novel TFC RO membranes with high permselectivity and anti-biofouling property can be obtained by employing HT nanoparticles as dopants in the PA layers and grafting silane coupling agents containing anti-biofouling functional groups on the membrane surface. Quaternary ammonium groups have potent anti-biofouling activity and were effective against various microorganisms. Its effect could be related to the harmful interactions between positively charged quaternary nitrogen and the head groups of acidic phospholipids with negative charges in microorganism membranes (Díez et al., 2020). Hence, it could be applied as an efficient strategy to use silane coupling agents containing quaternary ammonium to graft HT-incorporated TFN RO membranes.

Inspired by the properties of HT nanoparticles and silane coupling agents containing quaternary ammonium, this work aimed to develop novel RO membranes with prolonged and stable high performance by improving the original permselectivity and anti-biofouling property simultaneously. First, the Mg-Al-CO_3 HT nanoparticles were incorporated in PA layers during interfacial polymerization by dispersing in organic solutions. On the one hand, HT provided water transport channels and improved the water flux of the obtained membranes. On the other hand, the HT nanoparticles acted as bonding sites for functional groups grafting, avoiding the destruction of the PA matrix. Then, the toxic-free anti-biofouling agent dimethyloctadecyl[3-(trimethoxysilyl)propyl]ammonium chloride (DMOTPAC), which was usually used in the field of textiles, was involved in functionalizing the membranes. The advantages of nanoparticles incorporation and anti-biofouling grafting could be integrated by the method mentioned above. HT incorporation could compensate for the water flux loss caused by the following grafting reaction. The DMOTPAC on the membrane surface could provide extra anti-biofouling capacity. In addition, the grafting agent could react with HT rather than PA, which protects the PA matrix from damage. To the best of our knowledge, it has not been reported to build covalent bonds between DMOTPAC and HT nanoparticles embedded in PA matrix to obtain RO membranes with both high permselectivity and anti-biofouling properties.

In this work, the RO membranes were modified by HT incorporation and DMOTPAC grafting. The DMOTPAC concentration in grafting solution was varied to tune the properties of modified membranes. The surface morphology of the membranes was characterized, and the existence of nanoparticles in PA layers was verified. The membranes' chemical structure, surface charge and hydrophilicity were investigated by ATR-FTIR, XPS, zeta potential and contact angle. The water flux and salt rejection were measured to investigate the permselectivity of the membranes. Positively charged lysozyme and negatively charged BSA were used as model pollutants to evaluate the anti-fouling property of the membranes. Sterilization experiments of two model microorganisms, *E. coli* and *B. subtilis* evaluated the membranes' antimicrobial properties.

2 Materials and methods

2.1 Materials

Metaphenylene diamine (MPD, 99%, ACROS, Belgium), 10-camphor sulfonic acid (CSA, 98%, TCI, Tokyo, Japan), Triethylamine (TEA, AR, Fengchuan, Tianjin, China), Trimesoyl chloride (TMC, 99%, J&K Scientific, Beijing, China) and n-hexane (AR, Kemiou, Tianjin, China) were used to fabricate RO membranes. $Al(NO_3)_3 \cdot 9H_2O$ (AR, Sigma-Aldrich, Shanghai, China), $Mg(NO_3)_2 \cdot 6H_2O$ ($\geqslant$99.8%, Dongfang chemical plant, Beijing, China), Na_2CO_3 (AR, Fengchuan, Tianjin, China), NaOH (AR, Fengchuan, Tianjin, China) and methanol (AR, Kemiou, Tianjin, China) were used to prepare Mg-Al-CO_3 HT nanoparticles. Dimethyloctadecyl[3-(trimethoxysilyl)propyl]ammonium chloride (DMOTPAC, 60 wt% in methanol, Sigma-Aldrich, Shanghai, China) and methyl (AR, Kemiou, Tianjin, China) were used for anti-biofouling grafting. Lysozyme ($\geqslant$20000 U/mg, Sigma-Aldrich, Shanghai, China) and bovine serum albumin (BSA, Standard, Solarbio, Beijing, China) were employed to test the anti-biofouling properties of membranes. *Escherichia coli* (*E. coli*, China Center of Industrial Culture Collection, Beijing, China) and Bacillus subtilis (*B. subtilis*, Center of Industrial Culture Collection, Beijing, China) were employed to evaluate the antimicrobial property (a kind of biofouling) of the membranes. Live/dead bacteria staining kit (Yeasem Biotechnology, Shanghai, China) was used to stain bacteria on the membrane surface. Home-made ultrafiltration membranes consisted of polysulfone porous layer and non-woven fabrics support were used as substrates for RO membrane preparation. Deionized (DI) water was used for membrane preparation and characterization.

2.2 Synthesis of HT

The hydrothermal synthesis was used to prepare HT nanoparticles. The procedure has been described in our previous work (Tian et al., 2020).

2.3 Fabrification and modification of RO membranes

The interfacial polymerization (IP) method was used to prepare PA RO membranes. First, the surface of ultrafiltration substrates was covered with aqueous solution containing MPD (2.0 wt%), TEA (1.1 wt%) and CSA (2.3 wt%) for 1 min. Then, the aqueous solution on the

substrate surface was removed by air-knife. In the next step, the substrate surface was covered with an organic solution containing TMC (0.1 wt%) in n-hexane for 1 min to polymerise TMC and MPD. Finally, the as-obtained membrane was heated at 80°C for 5 min. The pristine membrane was denoted as PA-pristine. In a similar procedure, HT incorporated TFN RO membranes were obtained by scattering nanoparticles into the organic solution. After adding HT into n-hexane, the solution was stirred for 0.5 h and ultrasonically dispersed for 1 h. TMC was added in the last step. The organic solution was poured on the MPD-loaded substrate surface, and HT was incorporated into the as-produced PA layer during interfacial polymerization.

Surface modification of the membranes was conducted adopting a facile chemical coupling method. DMOTPAC was dissolved in methanol with different concentrations (0.02%, 0.06%, 0.10% and 0.50%). The grafting solution was poured on the surface of the as-obtained TFN RO membranes fixed by a sealed frame. The membrane surface was covered with grafting solution at 25°C for 3 h to allow the reaction. The as-modified membranes were named PA-HT-0.02, PA-HT-0.06, PA-HT-0.10 and PA-HT-0.50, according to the concentration of DMOTPAC. Pure methanol (without DMOTPAC) was also used to obtain the "reference" membrane PA-HT-0.

2.4 Characterization of HT nanoparticles and membranes

The chemical structure of HT nanoparticles was studied by ATR-FTIR (iS50, Nicolet, USA). The crystal structure of HT nanoparticles was investigated by XRD (Miniflex 600, Regaku, Japan). The morphology of HT nanoparticles was observed by SEM (Nova Nano450, FEI, USA) and AFM (SmartSPM-1000, AIST-NT, USA)

The surface appearance of RO membranes was investigated by SEM (SU3500, Hitachi, Japan). To verify the successful incorporation of HT nanoparticles, the cross-section of RO membranes was examined by TEM (Tecnai G2 F30, FEI, USA). For TEM analyses, the sample preparation of the membrane procedure was similar to that described by Lin et al. (Lin et al., 2016). RO membranes' chemical structure was studied by ATR-FTIR (iS50, Nicolet, USA) spectroscopy and XPS (ESCALAB 250Xi, Thermo Scientific, USA). RO membranes' surface zeta potential values were measured using a zeta potential analyzer (SurPASS, Anton Paar, Austria). The hydrophilicity of the membranes was measured by a goniometer (JC2000D2, Zhongchen, Shanghai, China). The surface roughness was investigated by AFM (SmartSPM-1000, AIST-NT, USA) in a tapping model.

2.5 Permselectivity testing of RO membranes

The membrane permselectivity was evuated by testing flux and rejection. The as-prepared aqueous solution containing 2000 mg/L NaCl was used as feed. Before testing, membranes went through a prepressing process (1.55 MPa for 0.5 h) to reach stable water flux. Afterwards, the permeated water rejection was calculated using the equations detailed in our previous work (Tian et al., 2020).

2.6 Anti-biofouling testing of RO membranes

A cyclic procedure consisted of fouling and rinse was performed to investigate the anti-biofouling performance of membranes (Zhang et al., 2020). Lysozyme and BSA were used as positively and negatively charged model pollutants, respectively. Before the test, RO membranes were subjected to a pressure of 1.55 MPa using DI water to reach a stable state. Then an aqueous solution containing 2000 mg/L NaCl and 500 mg/L lysozyme or BSA was used as feed solution. The initial flux was denoted as J_0. The water flux was measured every 30 min and denoted as J. The normalized flux values (J/J_0) were calculated to estimate the anti-biofouling property. After 5-h fouling, the fouled membrane was rinsed in situ with DI water for 1 h. The present investigation performed the fouling-rinse cycle 3 times to mimic the actual application.

The amount of proteins including lysozyme and BSA adsorbed on pristine RO membrane and the modified membrane was quantified using static adsorption tests. Different membranes (PA-pristine, PA-HT-0 and PA-HT-0.06) were fixed by sealed frames, and then 150 mL protein solutions (0.5 g/L) were poured onto the membrane surface. The effective contact area was 456 cm^2. The static adsorption tests lasted for 3 h. The adsorbed protein amount was calculated from the protein concentration in the solutions before and after the static adsorption test, using a UV-Vis spectrophotometer at a wavelength of 280 nm (SPECORD 210PLUS, Analytik Jena, Germany).

Antimicrobial performance (a kind anti-biofouling property) of membranes was investigated by sterilization experiment using two model microorganisms, *E. coli* and *B. subtilis*. Firstly, 60 μL bacteria suspension with a concentration of ≈10^6 CFU/mL was coated uniformly on the surface of the membrane sample, which was tapped on a 7.6 cm × 2.6 cm glass slide. The membrane surface was covered with another glass slide, and the pair was sealed. The samples were incubated at 37°C for 3 h. Afterwards, the membrane surface was rinsed thoroughly using 9 mL saline to collect bacterial cells, and 1 mL of the collected bacterial suspension was added into nutrient agar. After a 48-h incubation at 37°C, the agar plates were subjected to the counter (Scan 500, Interscience, France) to estimate the bacterial colony and the sterilization ratio.

To further investigate the anti-biofouling property of membranes, the living state of bacteria on the membrane surface was also tested. The bacteria suspensions were diluted until the absorbancy reached about 0.1 at 600 nm wavelength measured by spectrophotometer (Genesys30, Thermofisher, USA). RO membranes were fixed on the

bottom of a 6-well sterile plate and 5 mL bacteria suspension was added into each well. After a 24-h incubation at 37°C, the membrane surface was rinsed and stained using live/dead bacteria staining kit. The samples were washed with normal saline, separated from sterile plate and examined using CLSM (LSM800, Zeiss, Germany).

3 Results and discussion

3.1 Investigations of HT nanoparticles

The morpho-structural properties of HT nanoparticles were investigated by SEM, XRD and AFM (Fig. 1). It was found from the SEM micrograph that HT nanoparticles exhibited a thin nanosheet shape (Fig. 1(a)), which is typical for HT nanoparticles.

The diffraction peaks were observed at 11.4°, 22.9°, 34.5°, 38.6°, 45.9°, 60.5° and 61.8°, which were assigned to the (003), (006), (009), (015), (018), (110) and (113) planes, respectively (Fig. 1(b)). The peaks (003), (006), (009), (015), (018), (110) and (113) matched well with the already published XRD pattern of some HT nanoparticles, demonstrating that the obtained HT nanoparticles were well crystallized (Liao et al., 2015). Bragg equation ($n\lambda = 2d\sin\theta$) was used to calculate the basal spacing of hydrotalcite (Yang et al., 2016). The equation describes the relationship among the order of reflection n, the wavelength λ, the spacing d and the diffraction angle θ. In the crystal structure of HT, the first order ($n = 1$) reflection and X-ray pattern d_{003} correspond to the spacing. The wavelength of the X-ray used was 0.154 nm. The basal spacing of the nanoparticles was calculated to be 0.78 nm.

The AFM image shown in Fig. 1(c) revealed that the lateral size of HT was ≈200 nm with a smooth surface. The structure was confirmed by the platform in the height profile (Fig. 1(d)). The thickness of HT nanosheets was ≈25 nm.

3.2 Properties of RO membranes

3.2.1 Surface properties of RO membranes

Figure 2 presents the fabrication of HT embedded RO membrane and the grafting process of DMOTPAC on the mixed matrix membrane. An integrated separation layer with HT nanoparticles was formed for salt rejection. Due to

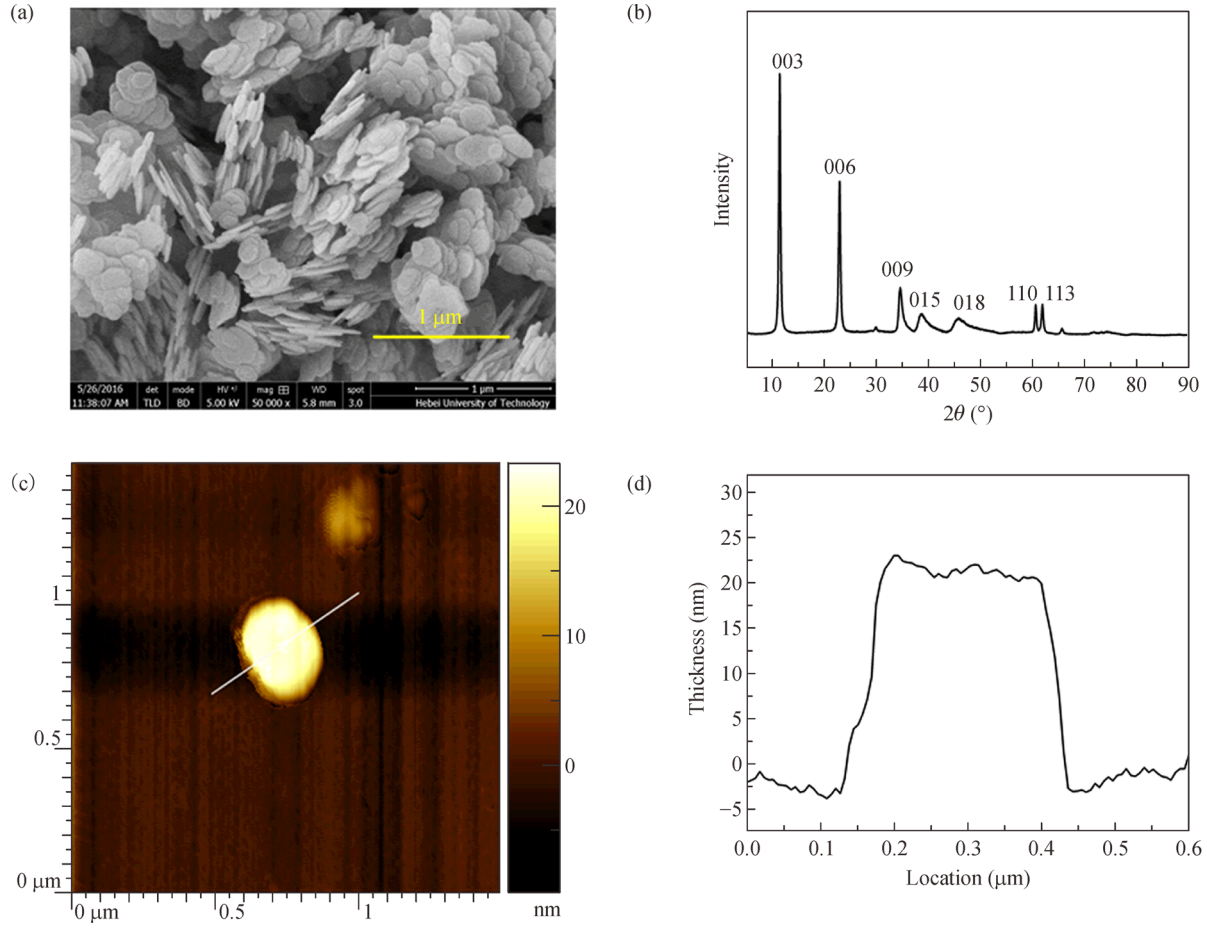

Fig. 1 Characterizations of HT nanoparticles: (a) SEM micrograph; (b) X-ray diffraction pattern; (c) AFM image; (d) height profile.

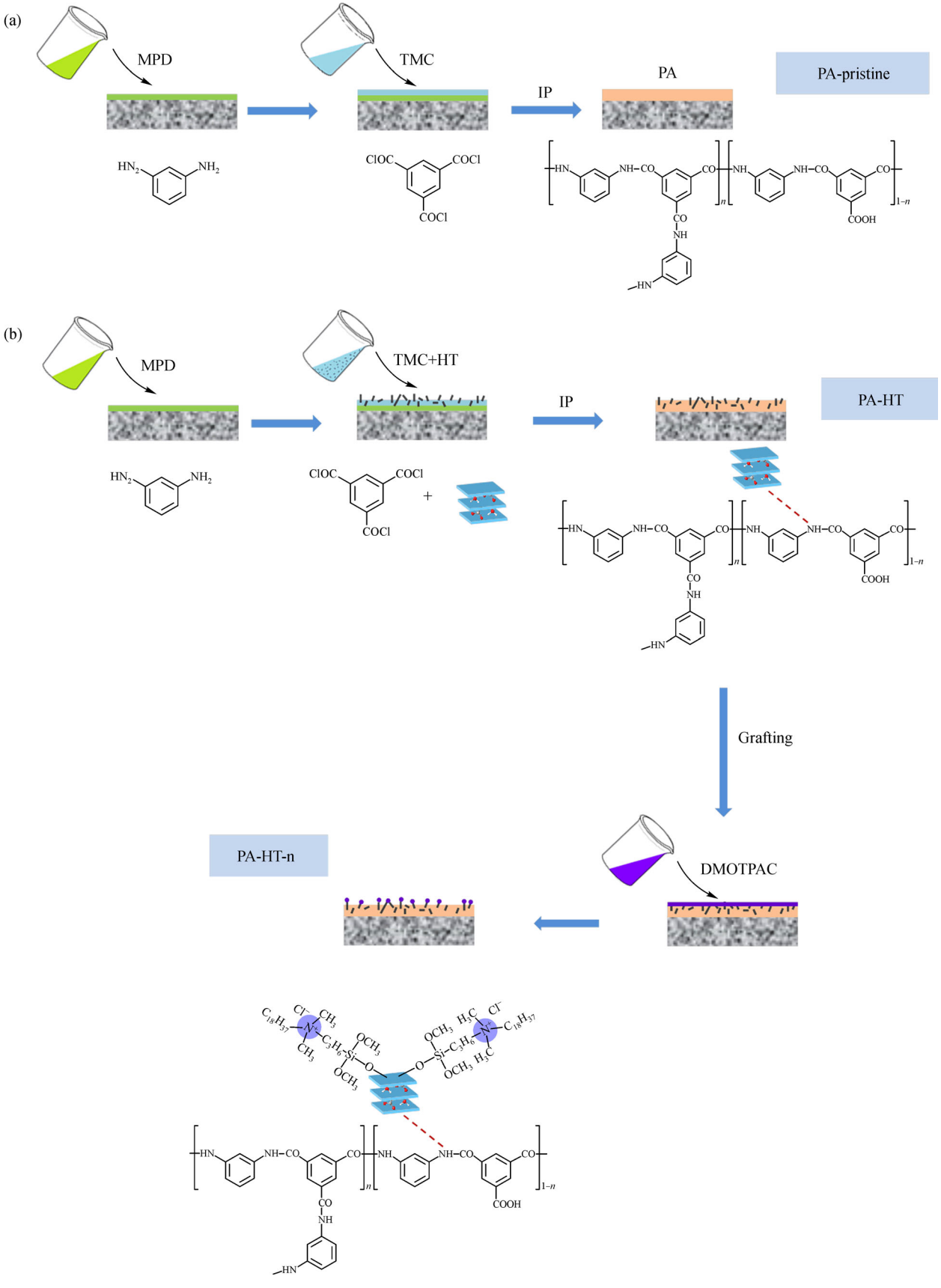

Fig. 2 Schematic illustration of membrane preparation: (a) PA-pristine; (b) modified membrane.

the presence of hydroxyls on the host layers, HT nanoparticles and PA matrix were combined with hydrogen bonding to form a relatively strong force besides van der Waals force (Shen et al., 2018). The hydroxyls on HT could form hydrogen bonding with amide and carboxyls in the PA matrix. As shown in Fig. 2, quaternary ammonium terminated silane coupling agent was adopted to react with hydroxyl, which was designed to endow the membranes with anti-biofouling property. It should be kept in mind that the HT content (0.025 wt%) and reaction parameters were optimized to ensure the outstanding separation performance of the resulting RO membrane.

The as-obtained RO membranes were characterized, and the main properties are detailed in Fig. 3. In Fig. 3(a), all the RO membranes exhibited a ridge-and-valley surface appearance, the characteristic of RO membranes fabricated through the interfacial polymerization method (Ghosh et al., 2008). Similar surface morphologies indicated that HT incorporation and DMOTPAC grafting did not destroy the main structure of PA layers. The reaction of MPD and TMC determined the surface morphology of RO membranes during the interfacial polymerization process. MPD diffused into the miscible phase of organic and water, and interfacial polymerisation occurred to form PA. Due to the continuous diffusion of MPD through the initially formed PA, the PA layer further grew. HT incorporation and DMOTPAC grafting did not change the polymerization process, and hence the surface morphology of the membrane surface was not influenced.

To analyze the structure of the separate layers and the existence of HT nanoparticles in the PA matrix, the cross-sectional morphology of the RO membrane was investigated by TEM (Fig. 3(b)). Following the results observed with SEM, all the separation layers exhibit ridge-and-valley surface morphology and the main structure is unaffected by the HT incorporation and DMOTPAC grafting. HT nanoparticles could be directly observed from the TEM micrographs due to the dark and opaque appearance of the inorganic nanoparticles. Since all the modified membranes PA-HT-0.02, PA-HT-0.06, PA-HT-0.10 and PA-HT-0.50 have shown similar TEM images, only membrane PA-HT-0.06 is displayed as a representative. As shown in Fig. 3(b), HT was introduced into the PA matrix during an interfacial polymerization. The embedded HT could construct high-speed channels for water transport, while the particles outside could provide binding sites for DMOTPAC. Hence, the HT nanoparticles were efficiently utilized, and they could play a dual role, which could be beneficial to their applicability.

Figure 3(c) shows the FTIR spectra of RO membranes. The peaks at 1665, 1608, and 1542 cm^{-1} belong to the absorption of C = O stretching, hydrogen-bonded C = O stretching and N-H in-plane bending, respectively, which are typical for the PA matrix in the separation layer. The peak at 1239 cm^{-1} belongs to the absorption of benzene-O-benzene stretching, which is characteristic of polysulfone in the porous layer of substrate (Xu et al., 2013). Compared with the pristine membrane, the DMOTPAC-modified membranes show three new bands at 2925, 2849 and 1026 cm^{-1}. The peaks at 2925 and 2849 cm^{-1} were attributed to the C-H stretching vibrations in the alkyl groups (-CH_2- and -CH_3) of the grafted DMOTPAC (see Fig. 2) (Wang et al., 2019). The peak at 1026 cm^{-1} was assigned C-Si-O, and its intensity grew from PA-HT-0.02 to PA-HT-0.10 (Liu et al., 2020). These results indicated that DMOTPAC was successfully grafted on membrane surfaces. Moreover, the quantity of DMOTPAC grafted on membrane surface increased with the DMOTPAC content increase in the grafting solution. The existence of DMOTPAC on the RO membrane surface was further investigated by XPS. Figure 3(d) shows the XPS N1s spectra of the membrane PA-HT-0.06. The N1s adsorption could be resolved into the neutral peak (C-N and O = C-N) component at 400.0 eV and the charged peak component C-N^+ at 402.3 eV (Do et al., 2012; Meng et al., 2015). The C-N^+ peak component suggested the presence of quaternary ammonium, which confirms the successful grafting of DMOTPAC on the membrane surface.

The DMOTPAC modification was further investigated by characterizing the zeta potential (Fig. 3(e)). The isoelectric point can reflect the type and amount of charges on the membrane surface. The pristine membrane showed an isoelectric point of 3.12, which was the synergistic result of carboxylic acid group ionization and amine group protonation. The isoelectric point of PA-HT-0 slightly shifted toward a higher pH value, indicating the successful incorporation of HT nanoparticles. The positive charge amount increased by HT incorporation due to the positively charged property and the partial exposure of the nanoparticles, as described in Fig. 2 (Dong et al., 2015). After DMOTPAC grafting, the isoelectric point further shifted toward a higher pH value, indicating that DMOTPAC was successfully grafted on the membrane surface. The grafting density increased with the increase of DMOTPAC concentration in the grafting solution. The quaternary amine groups in DMOTPAC grafted on the surface of the membranes provided a positive charge (Xu et al., 2015).

The membrane surface hydrophilicity was evaluated using water contact angle measurements (Fig. 3(f)). The water contact angle slightly decreased after incorporating HT nanoparticles, suggesting an improvement of surface hydrophilicity. Moreover, the surface hydrophilicity was unchanged with DMOTPAC grafting as the membranes exhibited similar water contact angle values. It is already known that the contact angle of membranes is mainly affected by surface chemical composition. As there are hydroxyl groups on the host layers of HT nanoparticles, water molecules were preferentially adsorbed onto the surface of the mixed matrix RO membranes. The DMOTPAC molecules influenced the hydrophilicity of the surface in a complex way.

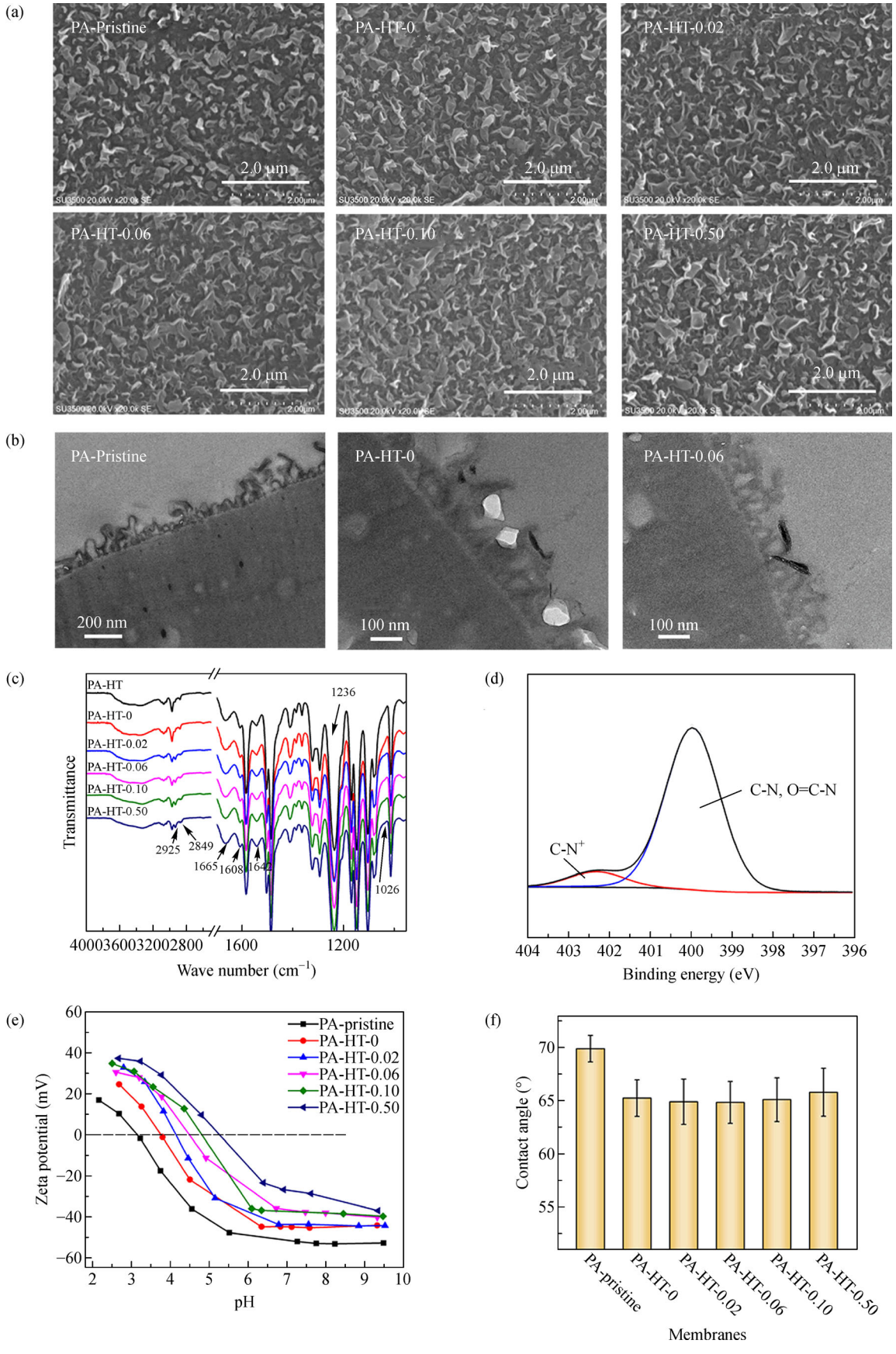

Fig. 3 Characterizations of RO membranes: (a) SEM micrographs; (b) TEM micrographs; (c) ATR-FTIR spectra; (d) N 1s spectra of DMOTPAC-grafted membrane; (e) zeta potentials; (f) contact angles.

On the one hand, the quaternary amine groups tend to improve the surface polarity, favoring water adsorption (Gao et al., 2015). On the other hand, the carbon chains are hydrophobic. The constant value of water contact angles could be ascribed to the comprehensive effects of these factors. Nonetheless, the modified membranes were relatively more hydrophilic than the unmodified membrane, conducive to water permeability improvement because of the high affinity between water and hydrophilic surfaces.

The AFM was used to investigate the influence of surface grafting on the roughness of RO membranes. Membrane surface parameters in terms of the average roughness (R_a) and root mean square roughness (R_{ms}) by AFM are collected in Table 1. The results suggest that R_a and R_{ms} values slightly increased with the HT incorporation and DMOTPAC grafting. The nanoparticles dispersed in organic solution tended to embed into PA layers, increasing surface roughness (Zhao et al., 2021). Hence, the R_a and R_{ms} values of PA-HT-0 are slightly higher than those of PA-pristine. The surface roughness increased with the increase of DMOTPAC concentration in the grafting solution. Because the DMOTPAC molecules randomly bonded to the exposed parts of HT nanoparticles (Zhang et al., 2020).

Table 1 Surface roughness of RO membranes

Membranes	R_a (nm)	R_{ms} (nm)
PA-pristine	56.1±1.9	70.0±2.3
PA-HT-0	59.2±1.7	74.0±2.0
PA-HT-0.02	62.5±2.9	77.6±3.2
PA-HT-0.06	65.7±3.3	81.6±3.4
PA-HT-0.10	67.2±3.1	84.5±5.5
PA-HT-0.50	71.0±2.2	88.5±4.0

3.2.2 Permselectivity of RO membranes

The effect of HT incorporation and DMOTPAC grafting on the membrane permselectivity was examined. Water flux and salt rejection were measured, according to Fig. 4. The HT incorporation improved the water flux of the RO membranes, which could be ascribed to the increase of the surface roughness, hydrophilicity enhancement and water channels constructed by HT. More significant surface roughness was obtained by incorporating HT, playing a positive role in water flux by providing a greater effective area for filtration. PA-HT-0 had a more hydrophilic surface, which had more vital water bonding ability and helped to improve water flux. Water channels offered by the pores of HT and the gaps between nanoparticles and PA matrix allowed a high-speed transfer of water, which improved water flux. After DMOTPAC grafting, the water flux gradually decreased with the concentration of DMOTPAC

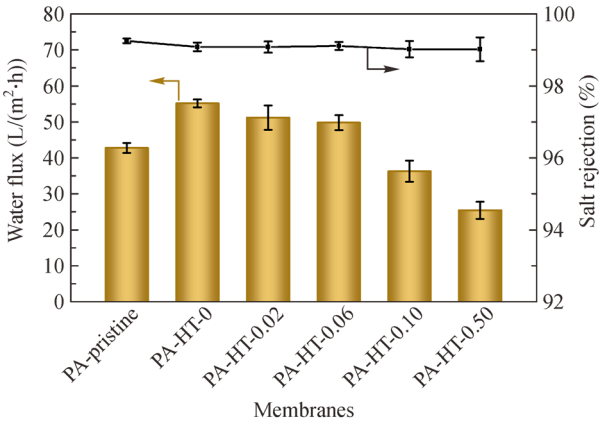

Fig. 4 Water flux and salt rejection of RO membranes.

in the grafting solution. The grafted DMOTPAC on the surface membrane forms an increased resistance to water transfer through the membrane, leading to a pressure drop (Xu et al., 2015). The water flux further decreases, verifying that many DMOTPAC molecules have been grafted on the membrane surface. The modified membranes showed an advantage in water flux when the DMOTPAC concentration was not more than 0.06 wt%. The water flux of PA-HT-0.06 was 49.8 L/m^2·h, which is 16.4% higher than that of PA-pristine (42.8 L/m^2·h). The introduction of HT nanoparticles could compensate for the mass transfer resistance resulted from the grafting layer to some degree. The as-modified membranes showed similar salt rejection as PA-pristine, indicating that the PA skin layer was not damaged by HT incorporation and DMOTPAC grafting. The salt rejection of PA-HT-0.06 was 99.1%, which is comparable to that of the pristine membrane. Hence, it is practical to maintain the relatively high water flux by nanoparticle incorporation when surface grafting was applied to functionalize the membranes. The HT nanoparticles were physically bonded with the PA matrix, and DMOTPAC molecules covalently bonded with the HT nanoparticles. The modification method presented in this work, integrating nanoparticle incorporation and anti-biofouling grafting, proved beneficial for achieving excellent selectivity.

3.2.3 Anti-biofouling property of RO membranes

Lysozyme and BSA were positively and negatively charged model pollutants to investigate the anti-biofouling properties (Xu et al., 2015; Zhang et al., 2020). The normalized water flux (the ratio of the current water flux during the fouling experiment to the initial value) was calculated to investigate the water flux variation. As shown in Fig. 5(a), the normalized water flux of the RO membranes decreased during the fouling procedure, regardless of lysozyme or BSA. This is because the

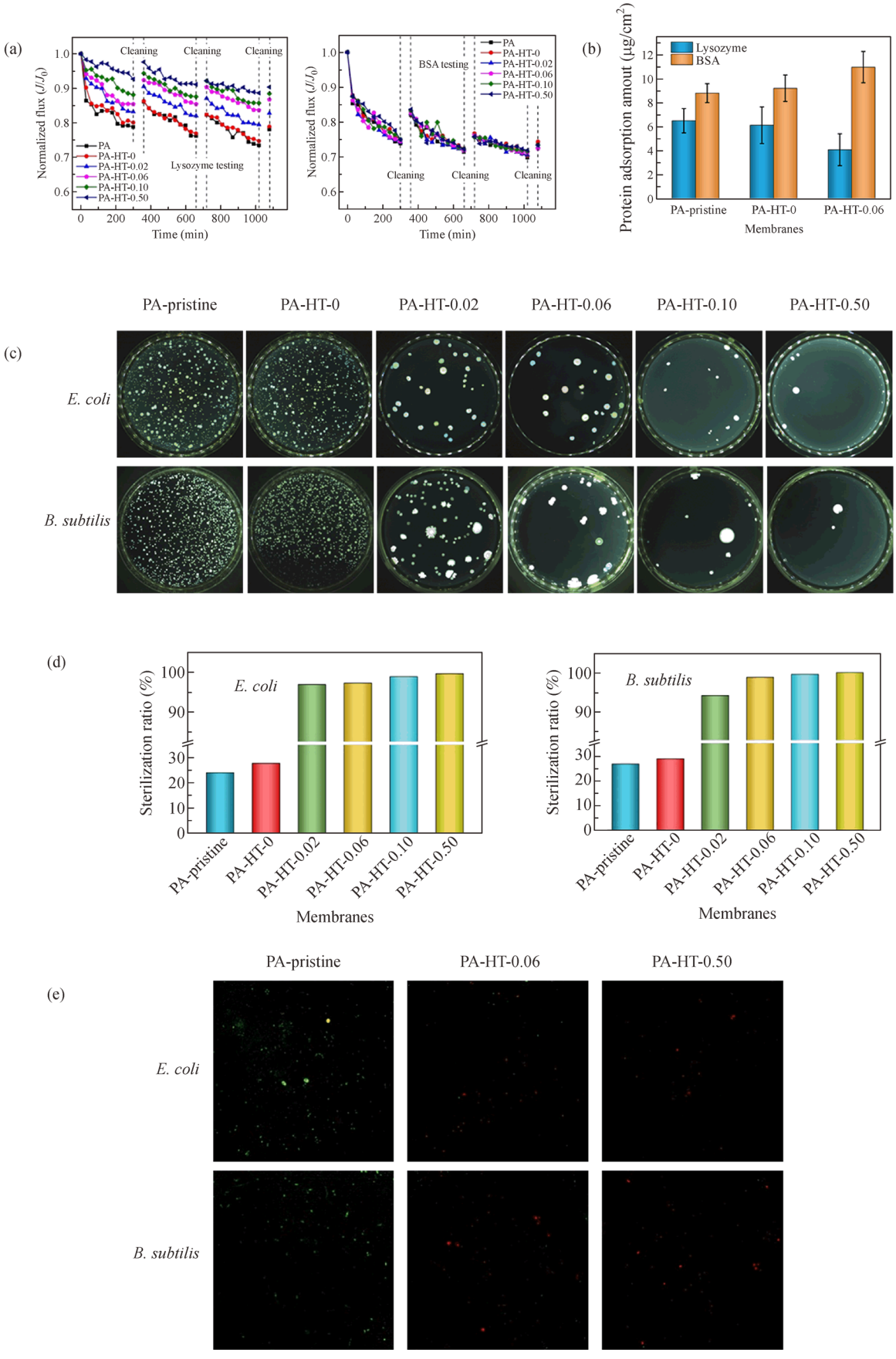

Fig. 5 Anti-biofouling properties of RO membranes: (a) normalized fluxes during fouling-rinse cycles; (b) static adsorption of proteins; (c) bacteria in contact with membrane surface after 3 h; (d) sterilization rates toward bacteria; (e) CLSM images of bacteria in contact with membrane surface after 24 h.

pollutants have a tendency to be physically adsorbed on the membrane surface, which increased resistance to the water across the membranes. During the testing of lysozyme fouling, the modified membranes exhibited lower flux decline and higher recovery ratios in each fouling-rinse cycle compared with the pristine membrane. In addition, this trend was more accentuated with the increase of the DMOTPAC concentration in the grafting solution. The third flux decline ratios of PA-pristine and PA-HT-0.06 were 26.5% and 16.3%, respectively. After three fouling-rinse cycles, the recovery ratios of PA-pristine and PA-HT-0.06 were 78.2% and 86.8%, respectively. The lower flux decline ratios and higher recovery ratios showed that the modification improved the anti-biofouling capacity against lysozyme. Fouling also occurred in the presence of BSA. The normalized flux dropped from 1.0 to ≈0.74 in the fouling procedure of the first cycle and then rose to ≈0.84 after rinse. After three fouling-rinse cycles, the recovery ratios of membranes was ≈0.74. The modified membranes exhibited similar normalized water flux variation with the pristine membrane, indicating that all the membranes had a similar anti-biofouling capacity against BSA.

The anti-biofouling capacity of membranes can be mainly ascribed to the surface properties of the membranes (Wang et al., 2017). Hydrophilicity, roughness and charge of surface influenced the interaction force between membrane surface and pollutants. The hydrophilic surface reduced the attraction between the membrane surface and hydrophobic organic pollutants. Meanwhile, water trended to bond to the hydrophilic membrane surface to form a barrier hindering pollutants from depositing. At the same time, pollutants were relatively easier to be trapped in the gaps of the ridge-and-valley structure on the rougher membrane surface, which enhanced the fouling on membranes with a rougher surface. The antifouling properties of membranes could be strengthened by the electrostatic repulsive force between membrane surface and pollutants when they had opposite charges. The modification endowed the membranes with a hydrophilic surface, facilitating a pure water layer formation on the surface, preventing pollutants from adsorbing and depositing onto the membrane surface (Wang et al., 2015). The membrane's surface roughness also influences the anti-biofouling properties. As the modification increased the surface roughness of the membranes, pollutants were prone to be trapped by the rough surface. Moreover, DMOTPAC grafting increased the quantity of positive charges on the surface of the modified membrane, which exhibited opposite electrostatic interactions to lysozyme and BSA. The electrostatic repulsion between positively charged lysozyme and membrane surface increased, reinforcing the anti-biofouling property toward lysozyme. However, the grafted DMOTPAC tended to attract BSA due to the opposite charges, weakening the repulsion between BSA and membrane surface. The modification's synergistic effects of hydrophilicity, charge and surface roughness led to the increased anti-biofouling property against lysozyme and the almost unchanged anti-biofouling property toward BSA.

The amounts of proteins on PA-pristine, PA-HT-0 and PA-HT-0.06 after static adsorption tests are presented in Fig. 5(b). The DMOTPAC-grafted membrane adsorbed less lysozyme and more BSA compared with the PA-pristine. This behavior is due to the positive charge of the DMOTPAC-grafted membrane surface, which repulsed the positively charged lysozyme but attracted the negative charged BSA. The results of static adsorption tests confirmed the presence of these interactions between BSA and the membrane surface.

The antimicrobial activity, an essential anti-biofouling property of the DMOTPAC-grafted membranes, was investigated by evaluating the growth of two types of model microorganisms on the membrane surface (Fig. 5(c)). The images show the colonies, representing the number of living bacteria in contact with the membrane surface after 3 h. As can be seen, the number of colonies decreased dramatically after being contacted with DMOTPAC-grafted membranes, which revealed an efficient antimicrobial property of these surfaces. Moreover, the corresponding sterilization ratios of the membranes were obtained (Fig. 5(d)). The sterilization rates of PA-pristine were ≈24.0% for *E. coli* and 26.7% for *B. subtilis*, which could be ascribed to the natural death of some bacteria during the experiment (Kang and Cao, 2012). Membranes after DMOTPAC modification showed higher sterilization rates. As to the membrane PA-HT-0.02, the sterilization rates were 96.9% toward *E. coli* and 94.0% toward *B. subtilis*. The values were further enhanced with the DMOTPAC concentration increase in the grafting solution. Considering the permselectivity and anti-biofouling property, PA-HT-0.06 was chosen as the best-performing membrane. The sterilization rates of PA-HT-0.06 toward *E. coli* and *B. subtilis* were 97.3% and 98.7%, respectively.

The antibacterial property of the RO membranes was mainly enhanced by DMOTPAC grafting, which is due to quaternary ammonium cations on the grafted DMOTPAC. It is generally accepted that a quaternary ammonium cation damages a bacteria cell because the charged nitrogen reaching the cell membrane surface can disrupt the balance of charge distribution. At the same time, the alkyl chains permeate the membrane and destroy cells' biochemical and physical properties (Wessels and Ingmer, 2013). The grafted DMOTPAC brought quaternary ammonium cations with antimicrobial property to the membrane surface. The quaternary ammonium cations damaged the bacteria and killed them. Hence, the modified membranes exhibited high sterilization rates.

To observe the inhibition process of bacteria, CLSM images of the membranes after contacting with bacteria were taken. Figure 5(e) shows the images of membranes

after a 24-h contact with *E. coli* or *B. subtilis*. The alive and dead bacteria show green and red appearance, respectively. A difference in both the live/dead state and the cell number of bacteria could be observed. Nearly all the bacteria on PA-pristine exhibited a green appearance, indicating that the bacteria were alive and the antibacterial activity of the pristine membrane was low. On the contrary, the bacteria on PA-HT-0.06 and PA-HT-0.50 were red, indicating bacteria were dead. Note that the total number of bacteria on the modified membranes was smaller than that on the pristine membrane, which could be ascribed to the loose construction of dead bacteria (Herzberg et al., 2009). The suitable anti-biofouling property to the biomass of modified membranes (see Fig. 5(a)) could benefit the exfoliation of dead bacteria from the membrane surface.

3.2.4 Further discussion on the modified membranes

Considering these results, a mechanism on the effects of HT incorporation and DMOTPAC grafting is proposed, as depicted in Fig. 6. The incorporation of HT contributes to the construction of high-speed water transport channels. Hence, the water flux was improved, which is designed to compensate for the loss caused by the following grafting. Moreover, the exposed areas of HT particles provide grafting sites for DMOTPAC. As mentioned before, quaternary ammonium cations in DMOTPAC kill bacteria, thus, extracellular polymeric substances will not be secreted. The construction of dead bacteria is loose, which is easy to peel. The grafting provides antimicrobial properties to the HT-incorporated membranes. Besides the advantages of nanoparticle incorporation and anti-biofouling grafting, the reaction between HT and DMOTPAC played an essential role in protecting the PA matrix from destruction. Consequently, the modified membranes possess high permselectivity and anti-biofouling property.

High permselectivity of the modified membranes helps to save energy and reduce cost during the reverse osmosis process. The anti-biofouling property protects membranes from performance degradation. Hence, the membranes could maintain prolonged stable high performance.

The amount of HT dispersed in the organic solution is limited due to the agglomeration of nanoparticles. Advanced technologies should be expected to overcome this problem, and the water flux and anti-biofouling properties of the as-modified membranes can be further improved.

4 Conclusions

In the present work, RO membranes possessing high permselectivity and anti-biofouling properties were prepared by HT incorporation and DMOTPAC grafting. HT was facilely introduced into the PA layers dispersed in organic solution. HT incorporation improved water flux, which could compensate for the water flux loss caused by the following grafting. Moreover, the exposed areas acted as grafting sites for DMOTPAC grafting. The water flux of PA-HT-0.06 was 49.8 L/m^2·h, which was 16.4% higher than that of the pristine membrane. As to the fouling of negatively charged lysozyme, the water flux recovery of the modified membrane was higher than that of the pristine membrane (e.g. 86.8% of PA-HT-0.06 compared to 78.2% of PA-pristine). The sterilization rate of PA-HT-0.06 for *E. coli* and *B. subtilis* were 97.3% and 98.7%. The mechanism of the combined effects of HT incorporation and DMOTPAC grafting was proposed. Considering these results, integrating nanoparticles incorporation and functional group grafting pledges the development of RO membranes with high permselectivity and anti-biofouling properties.

Acknowledgements This research was supported by the National Key Research and Development Program of China (Nos. 2018YFC0408002 and 2018YFE0196000), the Key Research Project of Shandong Province (China) (No. 2019JZZY010806), Shandong Provincial Natural Science Foundation (China) (ZR2020MB118), National Natural Science Foundation of China (Grant No. 21908257), the special Fund for Basic Scientific Research Business of Central Public Research Institutes (China) (Nos. K-JBYWF-2018-CR06, K-JBYWF-2018-HZ01) and the Natural Science Foundation of Tianjin (China) (No. 20JCZDJC00460).

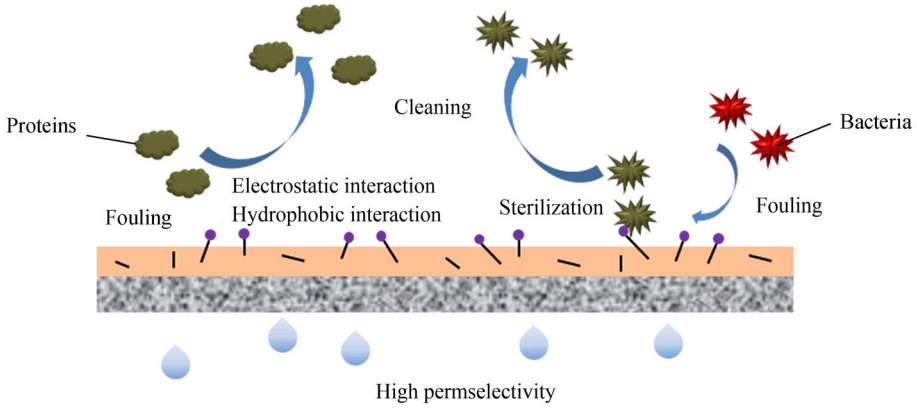

Fig. 6 Schematic representation of HT incorporation and DMOTPAC grafting.

References

Chae H R, Lee J, Lee C H, Kim I C, Park P K (2015). Graphene oxide-embedded thin-film composite reverse osmosis membrane with high flux, anti-biofouling, and chlorine resistance. Journal of Membrane Science, 483: 128–135

Dai R, Han H, Zhu Y, Wang X, Wang Z (2022). Tuning the primary selective nanochannels of MOF thin-film nanocomposite nanofiltration membranes for efficient removal of hydrophobic endocrine disrupting compounds. Frontiers of Environmental Science & Engineering, 16(4): 40

Díez B, Sotto A, Martín A, Arsuaga J, Rosal R (2020). Poly(vinyl chloride)-hyperbranched polyamidoamine ultrafiltration membranes with antifouling and antibiofouling properties. Reactive and Functional Polymers, 154: 104669

Do V T, Tang C Y, Reinhard M, Leckie J O (2012). Degradation of polyamide nanofiltration and reverse osmosis membranes by hypochlorite. Environmental Science & Technology, 46(2): 852–859

Dong H, Wu L, Zhang L, Chen H, Gao C (2015). Clay nanosheets as charged filler materials for high-performance and fouling-resistant thin film nanocomposite membranes. Journal of Membrane Science, 494: 92–103

Fane A G, Wang R, Hu M X (2015). Synthetic membranes for water purification: Status and future. Angewandte Chemie, 54(11): 3368–3386

Flemming H C, Schaule G, Griebe T, Schmitt J, Tamachkiarowa A (1997). Biofouling—the Achilles heel of membrane processes. Desalination, 113: 215–225

Gao C, Zhang M, Jiang Z, Liao J, Xie X, Huang T, Zhao J, Bai J, Pan F (2015). Preparation of a highly water-selective membrane for dehydration of acetone by incorporating potassium montmorillonite to construct ionized water channel. Chemical Engineering Science, 135: 461–471

Ghosh A K, Jeong B H, Huang X, Hoek E M V (2008). Impacts of reaction and curing conditions on polyamide composite reverse osmosis membrane properties. Journal of Membrane Science, 311: 34–45

Guo X, Li C, Li C, Wei T, Tong L, Shao H, Zhou Q, Wang L, Liao Y (2019). G-CNTs/PVDF mixed matrix membranes with improved antifouling properties and filtration performance. Frontiers of Environmental Science & Engineering, 13(6): 81

Hailemariam R H, Woo Y C, Damtie M M, Kim B C, Park K D, Choi J S (2020). Reverse osmosis membrane fabrication and modification technologies and future trends: A review. Advances in Colloid and Interface Science, 276: 102100

Henthorne L, Boysen B (2015). State-of-the-art of reverse osmosis desalination pretreatment. Desalination, 356: 129–139

Herzberg M, Kang S, Elimelech M (2009). Role of extracellular polymeric substances (EPS) in biofouling of reverse osmosis membranes. Environmental Science & Technology, 43(12): 4393–4398

Jeong B H, Hoek E M V, Yan Y, Subramani A, Huang X, Hurwitz G, Ghosh A K, Jawor A (2007). Interfacial polymerization of thin film nanocomposites: A new concept for reverse osmosis membranes. Journal of Membrane Science, 294: 1–7

Kang G D, Cao Y M (2012). Development of antifouling reverse osmosis membranes for water treatment: A review. Water Research, 46(3): 584–600

Kang G D, Gao C J, Chen W D, Jie X M, Cao Y M, Yuan Q (2007). Study on hypochlorite degradation of aromatic polyamide reverse osmosis membrane. Journal of Membrane Science, 300: 165–171

Liao J, Wang Z, Gao C, Wang M, Yan K, Xie X, Zhao S, Wang J, Wang S (2015). A high performance PVAm-HT membrane containing high-speed facilitated transport channels for CO_2 separation. Journal of Materials Chemistry. A, Materials for Energy and Sustainability, 3 (32): 16746–16761

Lin L, Lopez R, Ramon G Z, Coronell O (2016). Investigating the void structure of the polyamide active layers of thin-film composite membranes. Journal of Membrane Science, 497: 365–376

Liu W, Hu C, Zhang W, Liu Z, Shu J, Gu J (2020). Modification of birch wood surface with silane coupling agents for adhesion improvement of UV-curable ink. Progress in Organic Coatings, 148: 105833

Meng J, Zhang X, Ni L, Tang Z, Zhang Y, Zhang Y, Zhang W (2015). Antibacterial cellulose membrane via one-step covalent immobilization of ammonium/amine groups. Desalination, 359: 156–166

Saeki D, Tanimoto T, Matsuyama H (2014). Anti-biofouling of polyamide reverse osmosis membranes using phosphorylcholine polymer grafted by surface-initiated atom transfer radical polymerization. Desalination, 350: 21–27

Shen H, Wang S, Xu H, Zhou Y, Gao C (2018). Preparation of polyamide thin film nanocomposite membranes containing silica nanoparticles via an in-situ polymerization of $SiCl_4$ in organic solution. Journal of Membrane Science, 565: 145–156

Tian X, Cao Z, Wang J, Chen J, Wei Y (2020). Development of high-performance mixed matrix reverse osmosis membranes by incorporating aminosilane-modified hydrotalcite. RSC Advances, 10(10): 5648–5655

Wang F, Pi J, Li J Y, Song F, Feng R, Wang X L, Wang Y Z (2019). Highly-efficient separation of oil and water enabled by a silica nanoparticle coating with pH-triggered tunable surface wettability. Journal of Colloid and Interface Science, 557: 65–75

Wang J, Wang Z, Wang J, Wang S (2015). Improving the water flux and bio-fouling resistance of reverse osmosis (RO) membrane through surface modification by zwitterionic polymer. Journal of Membrane Science, 493: 188–199

Wang Y, Wang Z, Han X, Wang J, Wang S (2017). Improved flux and anti-biofouling performances of reverse osmosis membrane via surface layer-by-layer assembly. Journal of Membrane Science, 539: 403–411

Wessels S, Ingmer H (2013). Modes of action of three disinfectant active substances: A review. Regulatory Toxicology and Pharmacology, 67(3): 456–467

Xu J, Wang Z, Wang J, Wang S (2015). Positively charged aromatic polyamide reverse osmosis membrane with high anti-fouling property prepared by polyethylenimine grafting. Desalination, 365: 398–406

Xu J, Wang Z, Yu L, Wang J, Wang S (2013). A novel reverse osmosis membrane with regenerable anti-biofouling and chlorine resistant properties. Journal of Membrane Science, 435: 80–91

Yang C, Liao L, Lv G, Wu L, Mei L, Li Z (2016). Synthesis and characterization of Mn intercalated Mg-Al hydrotalcite. Journal of Colloid and Interface Science, 479(479): 115–120

Yin J, Deng B (2015). Polymer-matrix nanocomposite membranes for water treatment. Journal of Membrane Science, 479: 256–275

Zhang X, Huang H, Li Q, Yu H, Tian X, Zhao M, Zhang H (2020). Facile dual-functionalization of polyamide reverse osmosis membrane by a natural polypeptide to improve the antifouling and chlorine-resistant properties. Journal of Membrane Science, 604: 118044

Zhao Q, Zhao D L, Chung T S (2021). Thin-film nanocomposite membranes incorporated with defective ZIF-8 nanoparticles for brackish water and seawater desalination. Journal of Membrane Science, 625: 119158

Zhao X, Zhang R, Liu Y, He M, Su Y, Gao C, Jiang Z (2018). Antifouling membrane surface construction: Chemistry plays a critical role. Journal of Membrane Science, 551: 145–171

Zhu J, Hou J, Zhang Y, Tian M, He T, Liu J, Chen V (2018). Polymeric antimicrobial membranes enabled by nanomaterials for water treatment. Journal of Membrane Science, 550: 173–197